Energy Storage Materials 3 (2016) 77–84

Contents lists available at ScienceDirect

Energy Storage Materials

journal homepage: www.elsevier.com/locate/ensm

Li_2S_5-based ternary-salt electrolyte for robust lithium metal anode

Chen-Zi Zhao [a,1], Xin-Bing Cheng [a,1], Rui Zhang [a], Hong-Jie Peng [a], Jia-Qi Huang [a], Rui Ran [b], Zheng-Hong Huang [b], Fei Wei [a], Qiang Zhang [a,n]

[a] Beijing Key Laboratory of Green Chemical Reaction Engineering and Technology, Department of Chemical Engineering, Tsinghua University, Beijing 100084, China
[b] Department of Materials Science and Engineering, Tsinghua University, Beijing 100084, China

a r t i c l e i n f o

Article history:
Received 8 December 2015
Received in revised form
17 January 2016
Accepted 26 January 2016
Available online 2 February 2016

Keywords:
Lithium metal anode
Polysulfide
Dendrite
Lithium–sulfur batteries

a b s t r a c t

Li metal batteries (such as lithium–sulfur (Li–S) and lithium-air batteries) have been strongly considered as the promising candidates for the next-generation energy storage devices. Unfortunately, as the result of the notorious Li dendrite growth inherent in these batteries (upon repeated charge/discharge cycling), the concomitant serious safety concerns and low Coulombic efficiency have retarded their practical applications. Herein, we report a facile but effective strategy to in-situ construct a stable and compact solid electrolyte interphase (SEI) layer to protect Li deposits by the synergetic effect of Li_2S_5-based ternary-salt (LiTFSI–$LiNO_3$–Li_2S_5) electrolyte. LiTFSI affords a high Li^+ conductivity of the electrolyte in a working battery. The reactions between $LiNO_3$ and Li_2S_5 induce Li_2SO_3 formation, which is favorable to build protective SEI layer. Compared with routine LiTFSI mono-salt electrolyte, the Li_2S_5-based ternary-salt electrolyte renders Li metal anode (1) dendrite-free morphology, (2) improved Coulombic efficiency (94% compared with 60% in routine electrolyte), (3) suppressed polarization (26 mV at 5.0 mA cm^{-2} compared with 160 mV), and (4) prolonged lifespan (80 h compared with 20 h). These superior characteristics are attributed to the enhanced stability of the SEI layer by deliberately introducing the Li_2S_5 polysulfide as a pre-existing precursor, which, however, is always considered as an undesirable intermediate in Li–S batteries. Further development of this electrolyte enables practical applications for rechargeable lithium metal batteries, especially Li–S batteries.

& 2016 Elsevier B.V. All rights reserved.

1. Introduction

Lithium (Li) metal is regarded as the “Holy Grail” of battery technologies due to the high theoretical specific capacity (3860 mA h g^{-1}, which is 10 times that of commercial graphite anode) and the lowest redox potential (−3.040 V vs. the standard hydrogen electrode) [1–3]. The utilization of Li metal anodes can also eliminate the employment of current collectors in routine batteries with graphite, Si, Ge, and Sn anodes, hence dramatically boosting the energy density based on the total cell. Therefore, Li metal batteries (LMB), such as Li–sulfur (Li–S) [4–8] and Li-air ($Li–O_2$) batteries [6,9,10] with the theoretical energy density of 2600 and 3400 Wh kg^{-1}, respectively, could be promising candidates for the next-generation energy storage devices. Thus, it is not surprising that the exploitation of Li metal as a battery electrode has been a long-time dream since 1970s. However, they are still considered in their infancy due to the concomitant serious safety concerns and low Coulombic efficiency (CE), both of which are induced by the notorious Li dendrite growth.

Li dendrites are referred to branched or tree-like structures of the Li metal that is inhomogeneously deposited on the anode surface. Before accepting electrons and being reduced on the anode, Li ions inevitably pass through a solid layer between the electrolyte and anode, which was firstly named as the solid electrolyte interphase (SEI) by Peled in 1979 [11]. This electronic insulating and ionic conductive layer is derived from the electrochemical reactions between Li metal and electrolytes with the primary function of protecting the anode from further corrosion. As the result of the distinct Li^+ transfer properties, the SEI layer can serve as a redistributor of Li ions to avoid severe concentration gradient in the bulk electrolyte and thereby renders the homogeneous Li deposition to terminate Li dendrite growth in the initial nucleation stage. The dendrite suppression can be also effectively achieved if the shear modulus of the SEI layer is about twice that of the Li metal ($\sim 10^9$ Pa) [1]. Consequently, the composition, strength, and stability of the SEI layer are endowed pivotal roles on the Li depositing behavior. An ideal SEI should possess small thickness to decrease the consumption of electrolyte, high Li ionic conductivity to reduce the polarization, dense structure to

[n] Corresponding author.
E-mail address: zhang-qiang@mails.tsinghua.edu.cn (Q. Zhang).
[1] These authors contribute equally.

http://dx.doi.org/10.1016/j.ensm.2016.01.007
2405-8297/& 2016 Elsevier B.V. All rights reserved.

intercept the electrolyte molecules, and high elastic strength to mechanically suppress Li dendrite piercing. However, in most cases, SEI is unstable in the LMBs. The SEI either grows in thickness or becomes non-protective after several cycles, leading to rapid degradation of cell performance. Hence, a stable, uniform, and multifunctional SEI layer is of vital importance to inhibit uncontrolled dendritic and mossy Li growth.

Li metal is thermodynamically unstable in organic solvents. SEI layer is formed during the initial contact with electrolyte through parasitic reactions. Therefore, the modulation of electrolyte is one of the most efficient methods to stabilize SEI and to achieve a superior cycling stability of LMBs. Several electrolyte additives with higher reduction voltages than solvents and salts have been widely applied to reinforce the interfaces on Li metal, including lithium bis(fluorosulfonyl)imide (LiFSI) [12–14], halogenated salt [15], 1,1,2,2-tetrafluoroethyl-2,2,3,3-tetrafluoropropylether (TTE) [16], trace-amount H_2O [17], Cs^+ [18,19], concentrated electrolyte [14,20], etc. The in-situ formed SEI layer can well bring about the dendrite-free depositing behavior and prevent the electrolyte consumption. Other efficient approaches to build SEI layer include coating the Li electrode with an ex-situ formed protective layer (or 'artificial' SEI layer) [9,10,21–28], designing the anode structure to mediate SEI chemistry by nanoscale interfacial engineering [29–37], and chemical modification of separator [38–41]. These intense investigations highlight a series of strategies to prevent the dendrite growth and direct a promising attempt to propose future R&D trends.

Among various electrolyte additives, lithium nitrate ($LiNO_3$) is an important additive in the ether-based electrolyte (lithium bis (trifluoromethanesulfonyl)imide-1,3-dioxolane/1,2-dimethoxyethane, LiTFSI-DOL/DME) for Li–S batteries to effectively inhibit the side reactions between polysulfide intermediates and Li metal anode by constructing a stable SEI layer, which leads to a high CE of ~99% [42–46]. Further researches indicate that the stable and dense SEI layer is generated by the synergetic reactions between lithium polysulfides (LiPSs) and $LiNO_3$, rather than the sole $LiNO_3$, [47,48]. Cui and co-workers employed both LiPS (Li_2S_8) ([S]= 1.44 M) and $LiNO_3$ (5.0 wt%, ~0.75 M) as additives in the ether-based electrolyte (LiTFSI (1.0 M)-DOL/DME), enabling a synergetic effect to form a stable and uniform SEI layer on Li surface [49]. The SEI protecting layer can greatly minimize the electrolyte decomposition and prevent the shorting out of cells caused by dendrites. However, Li_2S_8 is metastable and easily disproportionates to elemental S and other lower-order LiPSs, which may take a toll on the SEI layer. A very high Li ion concentration of 2.11 M can even conceal the contribution of LiPS (Li_2S_8) for stable SEI formation on Li metal anode [14,20]. Actually, there are nearly eight kinds of LiPS intermediates varying from S to S chain length, namely Li_2S_8, Li_2S_7, Li_2S_6, Li_2S_5, Li_2S_4, Li_2S_3, Li_2S_2, and Li_2S [50,51]. The specific role of each LiPS is still tightly sealed. Therefore, the fantastic synergetic effect on the Li metal anode should be identified to the requested LiPS species at a low-concentration. This is beneficial for harvesting molecular insight on the complex reactions at the interfaces between Li metal and organic electrolyte and further provides ideal electrolyte based on the Li_2S_x additives for high-energy-density batteries with dendrite-free Li metal electrode.

In this contribution, we demonstrated the spontaneous reactions between different LiPS species and $LiNO_3$ to reinforce the SEI layer of Li metal anode. When coupling with $LiNO_3$, several LiPS species take an active role in suppressing the consumption of electrolyte. Especially, a small quantity of Li_2S_5 helps to build the Li_2S_5 ([S]=0.10 M)–$LiNO_3$ (1.0 wt%, ~0.15 M)-LiTFSI (1.0 M) ternary salt electrolyte and exerts superior cycling performance in Li metal anode with dendrite-free morphology and high-efficiency. Compared with the mono-salt (LiTFSI) and dual-salt (LiTFSI–$LiNO_3$) electrolyte, the cells with ternary-salt electrolyte exhibit a high CE of 4 90% at a large current density of 2.0 mA cm^{-2}. Even at a high deposited capacity of 4.0 mA h cm^{-2}, the ternary-salt electrolyte also maintains a very high CE above 95%. Such modification provides a mechanistic molecular-level understanding to inhibit the dendrite growth based on the interfacial chemistry.

2. Results and discussion

2.1. Selection of different LiPS species

Different LiPS species were synthesized from the stoichiometric reaction of Li_2S and S_8 in ether-based electrolyte. As the pure LiPS is hard be obtained due to the disproportionate and comproportionate reactions between different LiPSs, Li_2S_x is employed to indicate the average composition of LiPSs in the organic electrolyte. Although the exact sulfur specie of each soluble polysulfide solution is complicated and unknown, stoichiometric Li_2S_x is an appropriate indicator to distinguish them. With successive increased sulfur content in Li_2S_x (0.10 M [S]), LiPSs exhibit a transition of colors from milk white (Li_2S), dark yellow (Li_2S_2–Li_2S_4), to brownish red (Li_2S_5–Li_2S_8) and solubility from suspension (Li_2S and Li_2S_2) to solution (Li_2S_3–Li_2S_8) (Fig. 1a).

The cycling performance of Li plating and stripping in different LiPS species (i.e. Li_2S, Li_2S_2, Li_2S_3, Li_2S_4, Li_2S_5, Li_2S_6, Li_2S_7, and Li_2S_8)-based electrolytes, which is LiPS (0.10 M [S]), 1.0 wt% $LiNO_3$, 1.0 M LiTFSI in DOL/DME (1:1, in volume), was investigated in Cu|Li coin cells (Fig. 1b). Herein, one cycle is defined as that Li is firstly deposited on the Cu substrate and then is stripped from the Cu substrate. The CE is calculated from the ratio of the amount of Li stripped from the Cu substrate and the amount of Li plated onto it in one cycle.

At the concentration of 0.10 M ([S]), Li_2S_5 demonstrates the most superior cycling performance with a CE of 95%. However, other polysulfides lead to huge efficiency decay and fluctuation, which may be induced by the unstable and rapid-changing SEI layer during cycling. It also should be noted that the stability of protection from LiPSs varies a lot on the concentration. For ternary salt electrolyte with Li_2S_5, the concentration of 0.10 M [S] ([Li_2S_5]= 0.02 M, equivalently) is enough to guarantee CE 4 90% for early 100 cycles, while, for other kinds of polysulfides, the behaviors might be different. Consequently, the synergetic effect of LiPSs and $LiNO_3$ is determined by both the type and concentration of each LiPS.

2.2. Comparison between mono-/dual-/ternary-salt electrolytes

Li_2S_5-based electrolyte is selected as the probe system due to its excellent stability in storage period and superiority to improve CE among a variety of LiPS-based electrolytes. To demonstrate the critical role of the Li_2S_5, two control samples are prepared. One is mono-salt electrolyte (LiTFSI in DOL/DME) and the other is dual-salt electrolyte (LiTFSI–$LiNO_3$ in DOL/DME).

The CE of the Li metal electrode in the mono-salt electrolyte is with sharp oscillation and the efficiency dropped below 60% after 65th cycle at a low current density of 0.5 mA cm^{-2} (Fig. 2a), which may be attributed from the broken SEI and large dendrites after cycling (Fig. S1a). This indicates that a significant amount of the Li deposited on the substrate reacts with the electrolyte and cannot be fully recovered during the stripping process. As for the dual-salt electrolyte, it can maintain a relatively stable SEI layer with a CE of 94% at a low current density of 0.5 mA cm^{-2}. However, when the current density increases to 1.0 and 2.0 mA cm^{-2}, the CE of cells with dual-salt electrolyte exhibits large variation and fades rapidly. For the initial cycles, the CE can be maintained at 95% (1.0 mA cm^{-2}) and 92% (2.0 mA cm^{-2}). After 5 cycles, the dual-salt

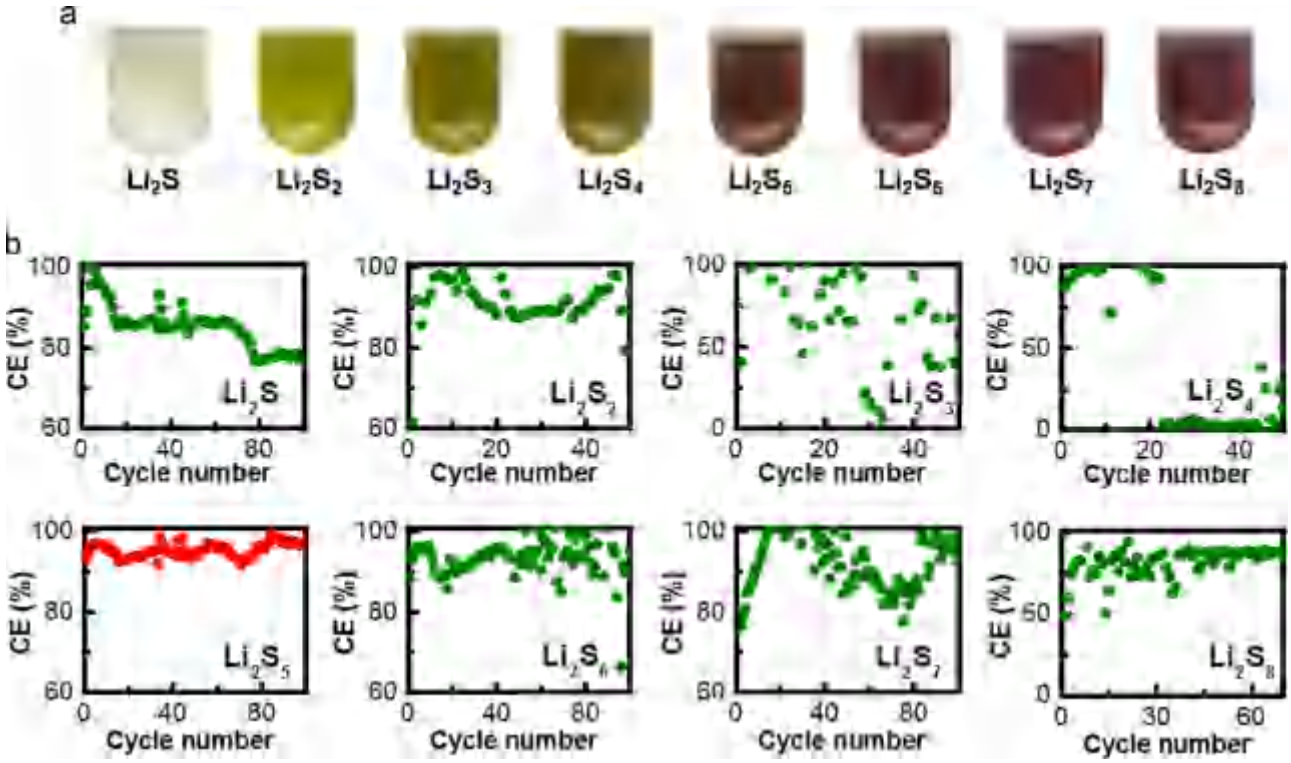

Fig. 1. Properties and cycling performances of ternary-salt electrolytes with different types of LiPSs. (a) Digital photographs of different ternary-salt electrolytes. (b) Coulombic efficiencies (CE) of the batteries with ternary-salt electrolytes based on different LiPSs. The current densities are all 0.5 mA cm^{-2} and the amount of Li deposited in each cycle is 0.5 mA h cm^{-2}.

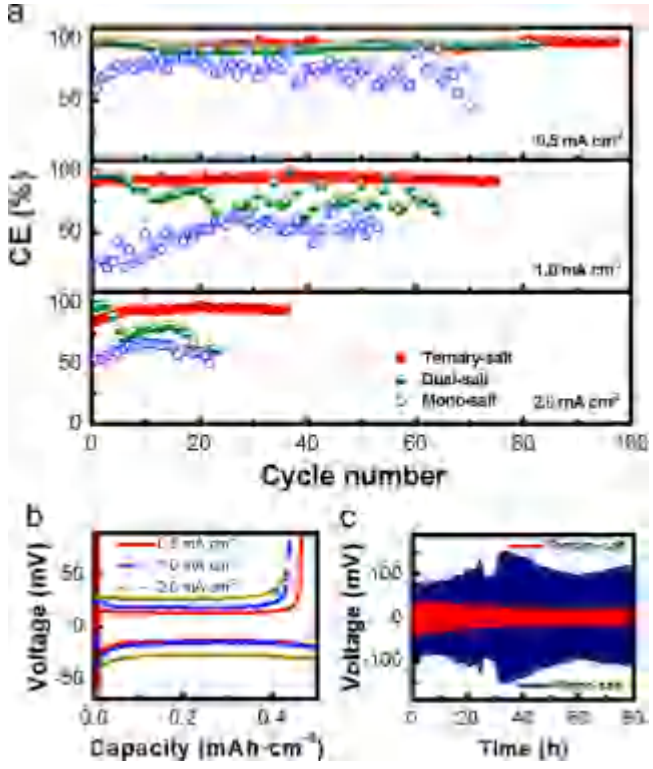

Fig. 2. Electrochemical performances of the cells with ternary-salt electrolyte. (a) CE of the cells with ternary-salt electrolytes (red, solid), dual-salt electrolytes (green, half-solid), and mono-salt electrolytes (blue, open) at different current densities. The amount of Li deposited in each cycle is 0.5 mA h cm^{-2}. (b) Polarization curves of the plating/stripping process for the ternary-salt electrolytes at different current densities. (c) Voltage versus time for a symmetric Li|Li cell where each half cycle lasts 6.0 min at a current density of 5.0 mA cm^{-2}.

induced SEI layer cannot be well maintained, due to the large Li dendrite growth at high-rate (Fig. S1b). The dehiscence of SEI layer results in large quantities of adverse reactions between the deposited Li metal and the electrolyte, thus leading to severe efficiency decay after 3–5 cycles. Therefore, the effect of $LiNO_3$ additive on the Li electrode at a low current density in initial 5 cycles is undoubtedly remarkable as previous studies validated [42]. Nevertheless, this positive effect is strongly limited. Fortunately, for cells with Li_2S_5-based ternary-salt electrolyte, the CE can stabilize at 95% for 100 cycles at 0.5 mA cm^{-2} and no dendrites are observed on the surface (Fig. S1c). Even at high current densities of 1.0 and 2.0 mA cm^{-2}, the cells still deliver a CE of 94% and 92%, respectively. The low CE at initial 5 cycles relative to that of dual-salt electrolyte is due to the consumed Li in the formation of LiS_x, $LiNO_x$ and Li_2SO_x to build the protective SEI layer. Consequently, we attribute the superior cycling performance relative to the mono-/dual-salt electrolytes to the synergy between Li_2S_5 and $LiNO_3$. Each one of them cannot afford efficiently protection alone (Fig. S2).

To investigate the electrochemical behavior of Li metal anode cycled at different rates, the charge–discharge curves are collected. The hysteresis is 26, 34, and 54 mV at a rate of 0.5, 1.0, and 2.0 mA cm^{-2}, respectively (Fig. 2b). Although the polarization of the cell increases with the rise of current density, Cu|Li cells with the Li_2S_5-based ternary-salt electrolyte can be cycled much more stable than the cells with mono-salt electrolyte and dual-salt electrolyte (Fig. S3). Even at a very high current density of 5.0 mA cm^{-2} in a symmetric Li|Li cell, the Li_2S_5-based ternary-salt electrolyte renders a dense SEI layer and maintains a stable cycling performance in 400 cycles (80 h), while the anode in the mono-salt electrolyte undergoes enormous volatility in the voltage–time curve (Figs. 2c and S4).

The hysteresis of Li|Li cell at a current density of 5.0 mA cm^{-2} is 23 mV, which is much lower than that of the mono-salt

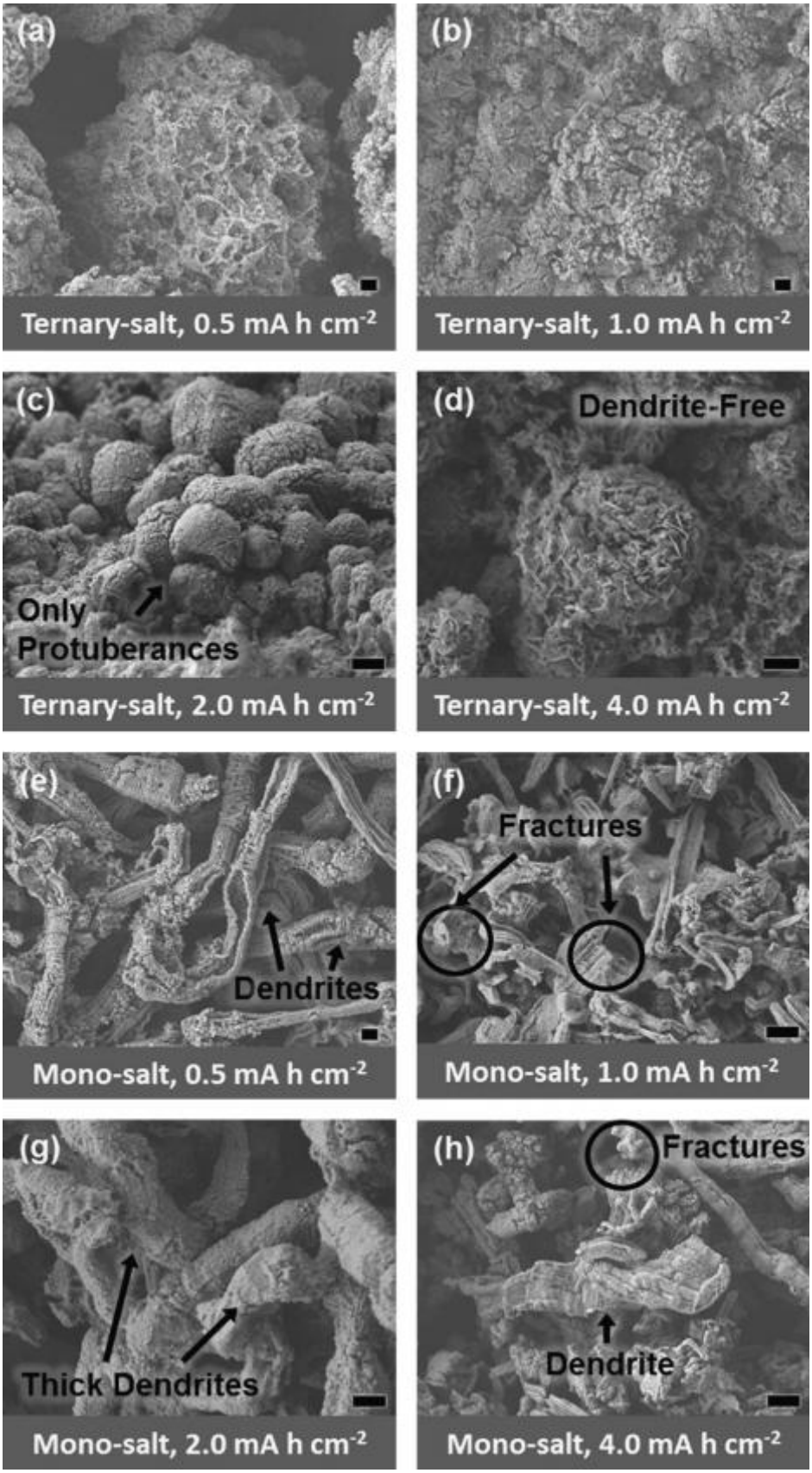

Fig. 3. Morphologies of the Li metal electrodes at different Li-plating capacities. SEM images of the Li electrodes in ternary-salt electrolytes at (a) 0.5 mA h cm^{-2}, (b) 1.0 mA h cm^{-2}, (c) 2.0 mA h cm^{-2}, (d) 4.0 mA h cm^{-2}; in mono-salt electrolytes at (e) 0.5 mA h cm^{-2}, (f) 1.0 mA h cm^{-2}, (g) 2.0 mA h cm^{-2}, (h) 4.0 mA h cm^{-2}. The current densities are 0.5 mA cm^{-2}. The scale bars are all 1 μm.

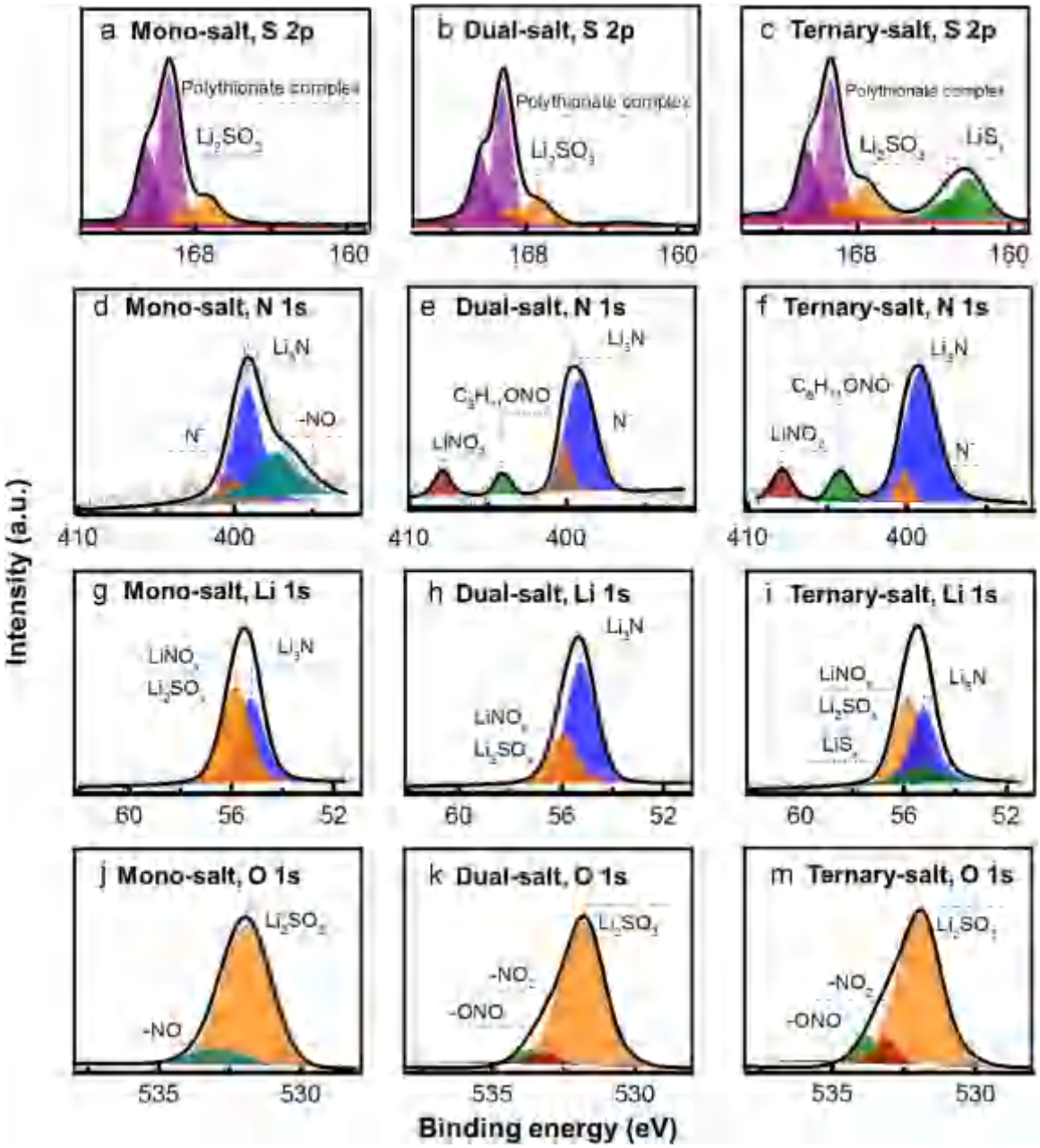

Fig. 4. Surface chemistry of the SEI layer. X-ray photoelectron spectroscopy (XPS) spectra of (a) mono-salt, S 2p, (b) dual-salt, S 2p, (c) ternary-salt, S 2p, (d) mono-salt, N 1s, (e) dual-salt, N 1s, (f) ternary-salt, N 1s, (g) mono-salt, Li 1s, (h) dual-salt, Li 1s, (i) ternary-salt, Li 1s, (j) mono-salt, O 1s, (k) dual-salt, O 1s, (m) ternary-salt, O 1s, from a Li electrode after cycling in mono/dual/ternary-salt electrolytes.

electrolyte. The erratic SEI layer of the mono-salt electrolyte results in large quantities of side reactions between Li dendrites and organic electrolyte. Therefore, a highly resistive SEI layer is formed and entangled within Li metal.

The layer dramatically increases the cell impedance and leads to cell degradation and failure, which is confirmed by the electrical impedance of the cells cycled at 5.0 mA cm^{-2}. As indicated in Fig. S5a, both the bulk and interfacial impedances increase sharply for cells with the mono-salt electrolyte compared to cells with ternary-salt electrolyte. An electric equivalent circuit is employed to interpret the Nyquist plots (Fig. S5b and Table S1), in which R_{Ω} indicates the ohmic resistance of electron transporting while R_{CT} represents the Li ion transfer resistance. The cells with ternary-salt electrolyte exhibit lower and much more stable values than that of mono-salt electrolyte in both R_{Ω} and R_{CT}, demonstrating an improved electron transport behavior within SEI for Li_2S_5-based ternary-salt electrolyte.

2.3. Cycling performance at high Li-plating capacity

Li depositing and stripping at high-capacity was conducted to further demonstrate the advantage of Li_2S_5-based ternary-salt electrolyte (Figs. 3 and S6). The cells with the Li_2S_5-based ternary-salt electrolyte maintain high average CEs of 95% and 96% at capacities of 0.5 and 1.0 mA h cm^{-2}, respectively. In contrast, when we use mono-salt electrolyte, the CEs drop to 74% and 75%, respectively. Even when the capacity is increased to 2.0 and 4.0 mA h cm^{-2}, which is even higher than what is used in practical applications, the average CE of ternary-salt electrolyte is 95% and 97%, respectively, whereas the CE of cells with the mono-salt electrolyte drops sharply. Although the efficiencies of the ternary-

salt electrolyte system display few fluctuations at higher capacity conditions, they are still above 90% and exhibit obvious amelioration compared with that of mono-salt electrolyte. This indicates that the cycling performance of Li metal electrode is significantly improved when Li_2S_5, $LiNO_3$, and LiTFSI are all present at high-capacity.

In Fig. 2a, ternary-salt electrolyte contributes prominently to improve CE, which implies a dendrite-free Li depositing behavior. Hence to forthrightly investigate the impact of Li_2S_5-based ternary-salt electrolyte on Li morphology, scanning electron microscope (SEM) images of Li deposits at different Li-plating capacities (0.5, 1.0, 2.0, and 4.0 mA h cm^{-2}) were collected (Fig. 3a–d). These images provide direct evidences that the Li_2S_5-based ternary-salt electrolyte strongly affects the morphology of Li metal electrode and the dendrite is eliminated.

With the ternary-salt electrolyte, there are no long whisker-like or bush-like dendrites in cycled Li electrode. Instead, only protuberances appear, which are the Li metal particles deposited under restriction. The protuberances on the surface become serried and then arranged to an even surface with the capacity increased from 0.5 to 4.0 mA h cm^{-2}. The dendrite-free morphology indicates a dense and stable SEI layer, which can be owed to complex reactions between ternary-salt electrolyte and Li metal. In contrast, the Li electrodes in the mono-salt electrolyte exhibit lots of bush-like dendrites at each capacity (Fig. 3e–h). The dendrites are slender at low-capacity of 0.5 mA h cm^{-2}. When the lithiation capacity increases, some of the dendrites are broken off due to the inhomogeneous dissolution of dendritic Li. The bush-like structure and pulverized Li is attributed from the unstable SEI layer in mono-salt electrolyte, which is incapable to offer valid protection of Li metal during depositing and stripping.

2.4. Surface chemistry of SEI layer

The SEI layer formed in the ternary-salt electrolyte has a thickness of ~40 nm as indicated in transmission electron microscopy (TEM) images and Auger electron Spectroscopy (AES) (Figs. S7 and S8), in which both the contrast and distribution of elements show evidently stratification. In Fig. S8, the upper layer contains more carbon than the lower layer. It is possible that there are organic layer (upper) and inorganic layer (lower) in SEI. X-ray photoelectron spectroscopy (XPS) analysis is employed to analyze the composition of the SEI layer. Fig. 4 manifests the XPS spectra of S 2p, N 1s, Li 1s, and O 1s for the Li metal electrode after electrochemical cycles in mono/dual/ternary-salt electrolyte. Compared with the SEI in mono-salt electrolyte, components such as –NO_2 and –ONO are detected, resulting from the reduction of $LiNO_3$. The –NO_2, –ONO, and Li_3N components on the Li surface are responsible for high CE in Li–S batteries with $LiNO_3$ additives. From the XPS spectra of the Li electrode in ternary-salt electrolyte (Fig. 4), S 2p can be assigned to lithium sulfide (Li_2S) and lithium sulfite (Li_2SO_x), respectively. The Li_2S is attributed to the spontaneous reaction between Li_2S_5 and Li metal. However, Li_2S_5 alone cannot effectively protect the anode (Fig. S2). Li_2SO_x is attributed to the redox reaction between Li_2S_5 and $LiNO_3$. Both Li 1s and O 1s spectrum confirm the coexistence of Li_2SO_x and LiN_xO_y in the SEI layer. The superior performance of SEI layer formed in ternary-salt electrolyte is attributed to the synergetic effect between the Li_2S_5 and $LiNO_3$ additives with the equilibrium of Li_2S_x, Li_2SO_x and LiN_xO_y in the surface chemistry.

Based on the XPS results, we firstly proposed a preliminary mechanism for the formation of the protective SEI film on Li metal anode in the LiTFSI–$LiNO_3$-Li_2S_5 ternary-salt electrolyte (Eqs. (1) and (2)).

$$LiNO_3 + Li^+ + e^- \rightarrow Li_2O + NO_2 \quad (1)$$

$$15Li_2O + 22NO_2 + S_5^{2-} \rightarrow 22NO_2^- + 5SO_3^{2-} + 30Li^+ \quad (2)$$

Herein, LiTFSI mainly plays the role of improving Li^+ conductivity [52,53], which is negligible during the formation of SEI layer. As $LiNO_3$ is a strong oxidizing agent, it is reduced firstly to NO_2 via obtaining Li^+ and e^- [48]. The NO_2 is much more active than $LiNO_3$ and undergoes spontaneous reaction with Li_2S_5, which generates Li_2SO_3, an important and beneficial component in the SEI layer [56].

2.5. Discussion

The ternary-salt electrolyte holds the superiority of inhibiting Li dendrite growth and improving CE for Li metal anodes, which is mainly ascribed to the synergistic effect of Li_2S_5, $LiNO_3$, and LiTFSI.

Among the three mentioned salts, LiTFSI is the most common salt as it offers ether-based electrolytes a proper conductivity and viscosity [54,55]. Nevertheless, LiTFSI alone cannot effectively protect Li metal due to the various $TFSI^-$ reduction products that precipitate on Li surfaces and form a heterogeneous film. The inhomogeneity may induce non-uniform current density distribution and eventually uneven Li deposit [13].

$LiNO_3$ has been introduced to stabilize the Li metal anode and achieved great success. However, $LiNO_3$ is rather unstable in the systems with a strong oxidizing property towards reductive agent such as Li. $LiNO_3$ undergoes progressive consumption till exhaustion in some extreme cycling conditions, such as high-rates and long cycles. As a result, the well-built SEI protecting layer induced by $LiNO_3$ additive alone is also easily corroded. $LiNO_3$ as a mono-additive are not suitable for sustainable cycling [44].

Accordingly, we choose Li_2S_5 and $LiNO_3$ as co-additives in the electrolyte. Li_2S_5 can effectively reduce the $LiNO_3$ into less oxidative $LiNO_2$ upon initial formation of SEI, differing from the controlled reaction between various LiPSs and Li metal anode in typical Li–S batteries.

The surface composition of SEI layer formed in Li_2S_5-based ternary-salt electrolyte includes Li_2SO_x, $LiNO_x$, Li_2S_x, etc, which are products of the synergistic reactions of Li_2S_5, $LiNO_3$, and Li metal (Fig. 4). These components in the SEI layer all render a positive effect on the cycling performance of Li metal anode to inhibit the dendrite growth and improve the CE [36,52,53].

The Li_2S_5-based ternary-salt electrolyte demonstrates a proof-of-concept for facilitating high-efficiency Li metal anode. The electrolyte system has several outstanding attributes:

(1) Superior cycling performance. The Li_2S_5-based ternary-salt electrolyte renders a stable, compact, and thin SEI layer to enable dendrite-free morphology, improved CE (from 60% to 94%), suppressed polarization (from 160 to 26 mV at 5.0 mA cm^{-2}), and prolonged lifespan (from 20 to 80 h);
(2) Enhanced safety assurance. The Li_2S_5-based ternary-salt electrolyte avoids the mass employment of $LiNO_3$ with strong oxidizing property and reduces the inflammability of the electrolyte;
(3) New sights into the role of different polysulfides. Polysulfides are mostly regarded as notorious intermediates in Li–S batteries [55,56]. Factually, some of them can work well to protect the Li metal anode when coupled with $LiNO_3$. The strategy proposed herein can shed new light on the polysulfide shuttle and Li metal protection through Li_2S_5 based ternary-salt electrolyte in Li–S batteries.
(4) SEI forming mechanism in polysulfide and $LiNO_3$ electrolyte. $LiNO_3$ is one of the most necessary additives in the Li–S batteries, which can improve CE from 80% to 99%. However, the exact mechanism is tightly sealed. The proposed mechanism herein provides new insights into the Li metal protection in

the Li–S and other metal batteries. The Li_2S_5-based ternary-salt electrolyte indicates a novel strategy to handle dendrite issues of lithium metal anodes, which could be applied to next-generation high-energy-density battery systems. Nevertheless, the critical role of Li_2S_5-based ternary-salt electrolyte is not eccentric because other polysulfides can also collaborate with $LiNO_3$ to present the protective role on the Li metal anode [49].

Apart from the type of polysulfide species, the concentration of polysulfide and the ratio of polysulfide to $LiNO_3$ also militate critically on the Li depositing morphology and cycling efficiency. Consequently, more elaborate design of the polysulfide based electrolyte is required to achieve a highly efficient LMBs with dendrite-free morphology, high CE, enhanced safety assurance and long lifespan.

3. Conclusion

Compact and dendrite-free Li metal can be plated/stripped from a Cu foil electrode at a high-rate and large lithiation capacity with a high Coulombic efficiency by employing the Li_2S_5-based ternary-salt (Li_2S_5–$LiNO_3$–LiTFSI) electrolyte. Li_2S_5-based ternary-salt electrolyte is beneficial to form dense and stable SEI layer, thus leading to the superior cycling performance. Compared with the Li metal anode in the mono-salt (LiTFSI) and dual-salt (LiTFSI–$LiNO_3$) electrolytes, the cells in ternary-salt electrolyte exhibited higher cycling efficiency (95%) and lower hysteresis (13.6 mV). Even at very high current density of 5.0 mA cm^{-2}, the SEI remained stable for more than 300 charging/discharging cycles. Besides, the morphology evolution of Li metal anode in ternary-salt electrolyte was observed to demonstrate the dendrite-free Li depositing morphology. The surface chemistry of the SEI layer was investigated and the forming mechanism was inferred to match the SEI structure. The Li_2S_5-based ternary electrolyte provides new sights into the safe and highly efficient utilization of Li metal electrodes for advanced energy storage applications. Beyond Li metal-based batteries, the strategies to modify electrolyte can be grafted to other battery-energy-storage-systems.

4. Experimental section

4.1. Preparation of the electrolytes

The mono-salt electrolyte was composed of 1.0 M LiTFSI and DOL/DME with volumetric ratio 1:1 (from Beijing Chemical Industry Group CO., LTD.). For $LiNO_3$–LiTFSI dual-salt electrolyte, only 1.0 wt% $LiNO_3$ (from Alfa Aesar) was added into the mono-salt electrolyte. Based on dual-salt electrolyte, Li_2S_x (x=1–8)–$LiNO_3$–LiTFSI electrolyte was prepared with the stoichiometric addition of Li_2S (from Alfa Aesar) and element sulfur, in which the concentration of sulfur element was fixed at 0.10 M ([S]=0.10 M), due to that the exact composition of each Li_2S_x solution is complicated and the existence of each S_x^{2-} cannot be well guaranteed. The Li_2S_5–LiTFSI dual-salt electrolyte was prepared with the addition of Li_2S_5 into mono-salt electrolyte.

4.2. Electrochemical measurements

The Li|electrolyte|Cu cells composing of lithium metal as the counter electrode and copper foil as the current collector of working electrode and Li|electrolyte|Li symmetrical cells composed of lithium metal in each electrode were employed. The cells were assembled with standard 2025 coin cells and STC24 dismountable cells (Shenzhen Kejingstar Technology Ltd.) in an Ar-filled glove box with O_2 and H_2O content below 1 ppm. The coin cells were monitored in galvanostatic mode within a voltage range of −0.5 to 1.5 V with Neware multichannel battery cycler. The EIS measurement (1–10^6 Hz) was performed on Solartron 1470E electrochemical workstation.

4.3. Characterization

The morphology of Li deposits was characterized by a JSM 7401F SEM operated at 3.0 kV and a JEM 2010 TEM operated at 120.0 kV. An Al-K_α radiation (72 W, 12 kV) at a pressure of 10^{-9} Torr was used to obtain the XPS spectra (XPS, ESCALAB 250Xi, Thermo Fisher Scientific Inc., USA). The diameter of the analyzed area was 400 μm. AES equipment is PHI-700, ULVAC-PHI, Japan. The batteries used for morphology and component characterization were assembled in STC24 dismountable cells in an Ar-filled glove box.

Appendix A. Supplementary material

Supplementary data associated with this article can be found in the online version at http://dx.doi.org/10.1016/j.ensm.2016.01.007.

References

[1] W. Xu, J. Wang, F. Ding, X. Chen, E. Nasybulin, Y. Zhang, J.-G. Zhang, Energy Environ. Sci. 7 (2014) 513–537.
[2] X.-B. Cheng, Q. Zhang, J. Mater. Chem. A 3 (2015) 7207–7209.
[3] X.-B. Cheng, R. Zhang, C.-Z. Zhao, F. Wei, J.-G. Zhang, Q. Zhang, Adv. Sci. 3 (2016) 1500213.
[4] M. Yu, R. Li, M. Wu, G. Shi, Energy Storage Mater. 1 (2015) 51–73.
[5] J. Liang, Z.-H. Sun, F. Li, H.-M. Cheng, Energy Storage Mater. 2 (2016) 76–106.
[6] W. Lv, Z. Li, Y. Deng, Q.-H. Yang, F. Kang, Energy Storage Mater. 2 (2016) 107–138.
[7] R.G. Cao, W. Xu, D.P. Lv, J. Xiao, J.G. Zhang, Adv. Energy Mater. 5 (2015) 1402273.
[8] G.M. Zhou, L. Li, D.W. Wang, X.Y. Shan, S.F. Pei, F. Li, H.M. Cheng, Adv. Mater. 27 (2015) 641–647.
[9] D.J. Lee, H. Lee, Y.-J. Kim, J.-K. Park, H.-T. Kim, Adv. Mater. 28 (2016) 857–863.
[10] Q.-C. Liu, J.-J. Xu, S. Yuan, Z.-W. Chang, D. Xu, Y.-B. Yin, L. Li, H.-X. Zhong, Y.-S. Jiang, J.-M. Yan, X.-B. Zhang, Adv. Mater. 27 (2015) 5241–5247.
[11] E. Peled, J. Electrochem. Soc. 126 (1979) 2047–2051.
[12] I.A. Shkrob, T.W. Marin, Y. Zhu, D.P. Abraham, J. Phys. Chem. C 118 (2014) 19661–19671.
[13] R. Miao, J. Yang, X. Feng, H. Jia, J. Wang, Y. Nuli, J. Power Sources 271 (2014) 291–297.
[14] J. Qian, W.A. Henderson, W. Xu, P. Bhattacharya, M. Engelhard, O. Borodin, J.-G. Zhang, Nat. Commun. 6 (2015) 6362.
[15] Y. Lu, Z. Tu, L.A. Archer, Nat. Mater. 13 (2014) 961–969.
[16] C. Zu, N. Azimi, Z. Zhang, A. Manthiram, J. Mater. Chem. A 3 (2015) 14864–14870.
[17] J. Qian, W. Xu, P. Bhattacharya, M. Engelhard, W.A. Henderson, Y. Zhang, J.-G. Zhang, Nano Energy 15 (2015) 135–144.
[18] F. Ding, W. Xu, G.L. Graff, J. Zhang, M.L. Sushko, X.L. Chen, Y.Y. Shao, M. H. Engelhard, Z.M. Nie, J. Xiao, X.J. Liu, P.V. Sushko, J. Liu, J.G. Zhang, J. Am. Chem. Soc. 135 (2013) 4450–4456.
[19] Y. Zhang, J. Qian, W. Xu, S.M. Russell, X. Chen, E. Nasybulin, P. Bhattacharya, M. H. Engelhard, D. Mei, R. Cao, F. Ding, A.V. Cresce, K. Xu, J.-G. Zhang, Nano Lett. 14 (2014) 6889–6896.
[20] L. Suo, Y.-S. Hu, H. Li, M. Armand, L. Chen, Nat. Commun. 4 (2013) 1481.
[21] G. Zheng, S.W. Lee, Z. Liang, H.-W. Lee, K. Yan, H. Yao, H. Wang, W. Li, S. Chu, Y. Cui, Nat. Nanotechnol. 9 (2014) 618–623.
[22] Y.J. Zhang, X.Y. Liu, W.Q. Bai, H. Tang, S.J. Shi, X.L. Wang, C.D. Gu, J.P. Tu, J. Power Sources 266 (2014) 43–50.
[23] K. Yan, H.-W. Lee, T. Gao, G. Zheng, H. Yao, H. Wang, Z. Lu, Y. Zhou, Z. Liang, Z. Liu, S. Chu, Y. Cui, Nano Lett. 14 (2014) 6016–6022.
[24] G. Ma, Z. Wen, M. Wu, C. Shen, Q. Wang, J. Jin, X. Wu, Chem. Commun. 50 (2014) 14209–14212.
[25] G. Ma, Z. Wen, Q. Wang, C. Shen, J. Jin, X. Wu, J. Mater. Chem. A 2 (2014) 19355–19359.
[26] Y.J. Zhang, W. Wang, H. Tang, W.Q. Bai, X. Ge, X.L. Wang, C.D. Gu, J.P. Tu, J. Power Sources 277 (2015) 304–311.
[27] H. Lee, D.J. Lee, Y.-J. Kim, J.-K. Park, H.-T. Kim, J. Power Sources 284 (2015) 103–108.

[28] E. Kazyak, K.N. Wood, N.P. Dasgupta, Chem. Mater. 27 (2015) 6457–6462.
[29] J. Heine, S. Krüger, C. Hartnig, U. Wietelmann, M. Winter, P. Bieker, Adv. Energy Mater. 4 (2014) 1300815.
[30] C. Huang, J. Xiao, Y. Shao, J. Zheng, W.D. Bennett, D. Lu, L.V. Saraf, M. Engelhard, L. Ji, J. Zhang, X. Li, G.L. Graff, J. Liu, Nat. Commun. 5 (2014) 3015.
[31] X. Zhang, W. Wang, A. Wang, Y. Huang, K. Yuan, Z. Yu, J. Qiu, Y. Yang, J. Mater. Chem. A 2 (2014) 11660–11665.
[32] X. Ji, D.-Y. Liu, D.G. Prendiville, Y. Zhang, X. Liu, G.D. Stucky, Nano Today 7 (2012) 10–20.
[33] R. Mukherjee, A.V. Thomas, D. Datta, E. Singh, J. Li, O. Eksik, V.B. Shenoy, N. Koratkar, Nat. Commun. 5 (2014) 3710.
[34] J.-S. Kim, D.W. Kim, H.T. Jung, J.W. Choi, Chem. Mater. 27 (2015) 2780–2787.
[35] X.B. Cheng, H.J. Peng, J.Q. Huang, F. Wei, Q. Zhang, Small 10 (2014) 4257–4263.
[36] X.-B. Cheng, H.-J. Peng, J.-Q. Huang, R. Zhang, C.-Z. Zhao, Q. Zhang, ACS Nano 9 (2015) 6373.
[37] C.-P. Yang, Y.-X. Yin, S.-F. Zhang, N.-W. Li, Y.-G. Guo, Nat. Commun. 6 (2015) 8058.
[38] X.W. Yu, Z.H. Bi, F. Zhao, A. Manthiram, ACS Appl. Mater. Interfaces 7 (2015) 16625–16631.
[39] W. Luo, L.H. Zhou, K. Fu, Z. Yang, J.Y. Wan, M. Manno, Y.G. Yao, H.L. Zhu, B. Yang, L.B. Hu, Nano Lett. 15 (2015) 6149–6154.
[40] W.K. Shin, A.G. Kannan, D.W. Kim, ACS Appl. Mater. Interfaces 7 (2015) 23700–23707.
[41] H.J. Peng, D.W. Wang, J.Q. Huang, X.B. Cheng, Z. Yuan, F. Wei, Q. Zhang, Adv. Sci. 3 (2016) 1500268.
[42] D. Aurbach, E. Pollak, R. Elazari, G. Salitra, C.S. Kelley, J. Affinito, J. Electrochem. Soc. 156 (2009) A694–A702.
[43] Y. Diao, K. Xie, S.Z. Xiong, X.B. Hong, J. Electrochem. Soc. 159 (2012) A1816–A1821.
[44] S.S. Zhang, Electrochimica Acta 70 (2012) 344–348.
[45] J. Guo, Z. Wen, M. Wu, J. Jin, Y. Liu, Electrochem. Commun. 51 (2015) 59–63.
[46] X. Liang, Z.Y. Wen, Y. Liu, M.F. Wu, J. Jin, H. Zhang, X.W. Wu, J. Power Sources 196 (2011) 9839–9843.
[47] S. Xiong, Y. Diao, X. Hong, Y. Chen, K. Xie, J. Electroanal. Chem. 719 (2014) 122–126.
[48] S. Xiong, K. Xie, Y. Diao, X. Hong, J. Power Sources 246 (2014) 840–845.
[49] W. Li, H. Yao, K. Yan, G. Zheng, Z. Liang, Y.-M. Chiang, Y. Cui, Nat. Commun. 6 (2015) 7436.
[50] M. Cuisinier, P.E. Cabelguen, B.D. Adams, A. Garsuch, M. Balasubramanian, L. F. Nazar, Energy Environ. Sci. 7 (2014) 2697–2705.
[51] M.-Q. Zhao, M. Sedran, Z. Ling, M.R. Lukatskaya, O. Mashtalir, M. Ghidiu, B. Dyatkin, D.J. Tallman, T. Djenizian, M.W. Barsoum, Y. Gogotsi, Angew. Chem. Int. Ed. 54 (2015) 4810–4814.
[52] K. Xu, Chem. Rev. 104 (2004) 4303–4418.
[53] K. Xu, Chem. Rev. 114 (2014) 11503–11618.
[54] E.G. Leggesse, J.-C. Jiang, J. Phys. Chem. A 116 (2012) 11025–11033.
[55] G. Zhou, E. Paek, G.S. Hwang, A. Manthiram, Nat. Commun. 6 (2015) 7760.
[56] J. Song, M.L. Gordin, T. Xu, S. Chen, Z. Yu, H. Sohn, J. Lu, Y. Ren, Y. Duan, D. Wang, Angew. Chem. Int. Ed. 54 (2015) 4325–4329.